Construction of 6-thioguanine and 6-mercaptopurine carriers based on βcyclodextrins and gold nanoparticles

Article *in* Carbohydrate Polymers · August 2017

DOI: 10.1016/j.carbpol.2017.08.102

CITATIONS
4

READS
124

7 authors, including:

Rodrigo Sierpe Bustamante
University of Chile
12 PUBLICATIONS **21** CITATIONS

SEE PROFILE

Marcelo J Kogan
University of Chile
117 PUBLICATIONS **2,746** CITATIONS

SEE PROFILE

Carbohydrate Polymers 177 (2017) 22–31

Contents lists available at ScienceDirect

Carbohydrate Polymers

journal homepage: www.elsevier.com/locate/carbpol

Research Paper

Construction of 6-thioguanine and 6-mercaptopurine carriers based on βcyclodextrins and gold nanoparticles

R. Sierpe[a,b,c], Michael Noyong[d], Ulrich Simon[d], D. Aguayo[e], J. Huerta[e], Marcelo J. Kogan[b,c], N. Yutronic[a,*]

[a] Departamento de Química, Facultad de Ciencias, Universidad de Chile, Las Palmeras #3425, Ñuñoa, Santiago, Chile
[b] Departamento de Química Farmacológica y Toxicológica, Facultad de Ciencias Químicas y Farmacéuticas, Universidad de Chile, Sergio Livingstone #1007, Independencia, Santiago, Chile
[c] Advanced Center for Chronic Diseases (ACCDiS), Sergio Livingstone #1007, Independencia, Santiago, Chile
[d] RWTH Aachen University, Institute of Inorganic Chemistry, Landoltweg 1a, D-52074 Aachen, Germany
[e] Center for Bioinformatics and Integrative Biology (CBIB), Facultad de Ciencias Biológicas, Universidad Andrés Bello, República 239, Santiago, Chile

ARTICLE INFO

Keywords:
Antineoplastic
Complexes
Nanotechnology
Sputtering
Drug delivery

ABSTRACT

As a novel strategy to overcome some of the therapeutic disadvantages of 6-thioguanine (TG) and 6-mercaptopurine (MP), we propose the inclusion of these drugs in βcyclodextrin (βCD) to form the complexes βCD-TG and βCD-MP, followed by subsequent interaction with gold nanoparticles (AuNPs), generating the ternary systems: βCD-TG-AuNPs and βCD-MP-AuNPs. This modification increased their solubility and improved their stability, betting by a site-specific transport due to their nanometric dimensions, among other advantages.

The formation of the complexes was confirmed using powder X-ray diffraction, thermogravimetric analysis and one and two-dimensional NMR. A theoretical study using DFT and molecular modelling was conducted to obtain the more stable tautomeric species of TG and MP in solution and confirm the proposed inclusion geometries. The deposition of AuNPs onto βCD-TG and βCD-MP *via* sputtering was confirmed by UV–vis spectroscopy. Subsequently, the ternary systems were characterized by TEM, FE-SEM and EDX to directly observe the deposited AuNPs and evaluate their sizes, size dispersion, and composition. Finally, the *in vitro* permeability of the ternary systems was studied using parallel artificial membrane permeability assay (PAMPA).

1. Introduction

The drugs 6-thioguanine (TG) and 6-mercaptopurine (MP) are analogues of guanine and adenine (see their structures in Fig. 1a and b) and are used clinically to treat acute lymphoblastic leukaemia (ALL) in children and other types of leukaemia (Erb, Harms, & Janka-Schaub, 1998). In addition, TG is used as an immunosuppressant in transplant surgery, and it has been shown to hinder HIV replication (Krynetskaia et al., 2001). MP is also used for Crohn's disease or together with methotrexate for leukaemia (Chande, Townsend, Parker, & MacDonald, 2016; Schmiegelow, Nielsen, Frandsen, & Nersting, 2014). The applications of TG and MP were discovered in 1951 by Gertrude B. Elion, who reported evidence that they could produce complete remission in children with ALL. These medications were approved by the Food and Drug Administration (FDA) just two years after the first synthesis (Elion, 2008). Despite their proven efficacy as antineoplastic agents, TG and MP have some therapeutic disadvantages. After oral administration, they exhibit poor absorption, reaching sufficient plasma concentrations after 10–12 h. Moreover, food can reduce their bioavailability to a considerable degree. These drugs are distributed throughout the body, preferably focusing on the bone marrow; they do not cross the blood-brain barrier, are widely metabolized in the liver and are excreted through the urine. Several research efforts have been directed towards modifying their structures and synthesizing new nucleoside analogues to promote more selective effects and increase these drugs' aqueous solubility (Bohon & De los Santos, 2003; Erb et al., 1998).

An interesting way to change the physicochemical properties of a drug is through subtle interactions that do not alter its chemical structure. This can be achieved *via* inclusion in cyclodextrin (CD) matrices, leading to new therapeutic approaches (Ceborska, 2014; Tiwari, Tiwari, & Rai, 2010; Zhang & Ma, 2013), even in cancer (Gidwani & Vyas, 2015). βcyclodextrin (βCD) is a cyclic oligosaccharide, is non-toxic, and consists of 7 glucose units linked by α(1–4) bonds, forming a truncated cone (see the structures in

* Corresponding author.
E-mail addresses: rsierpe@ciq.uchile.cl (R. Sierpe), mnoyong@ac.rwth-aachen.de (M. Noyong), usimon@ac.rwth-aachen.de (U. Simon), daniel.aguayo@unab.cl (D. Aguayo), j.huerta.bq@gmail.com (J. Huerta), mkogan@ciq.uchile.cl (M.J. Kogan), nyutroni@uchile.cl (N. Yutronic).

http://dx.doi.org/10.1016/j.carbpol.2017.08.102
Received 26 April 2017; Received in revised form 26 July 2017; Accepted 20 August 2017
Available online 25 August 2017
0144-8617/

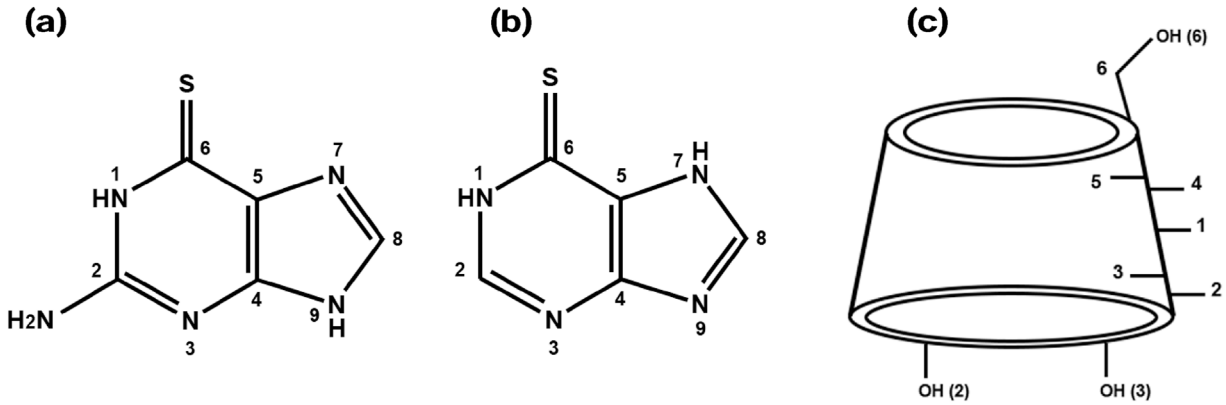

Fig. 1. Structures of (a) TG, (b) MP and (c) βCD with their respective proton assignments.

Fig. 1c) with a cavity diameter of 6–6.5 Å (Del Valle, 2004). Its inner cavity is partially hydrophobic, and its outer surface is hydrophilic. Thus, βCD is capable of including preferably non polar compounds, such as aliphatic chains, aromatic or heterocyclic compounds (Chen, Chang, & Gilson, 2004; Chen, Diao, & Zhang, 2006; Douhal, 2004; Makedonopoulou & Mavridis, 2000; Sierpe et al., 2015; Whang, Vendeix, Gracz, Gadsby, & Tonelli, 2007). βCD has been described in numerous research papers, patents and conference presentations, although most studies have focused on its pharmaceutical applications (Loftsson & Brewster, 2010). As a matrix, βCD has been widely used for drug delivery as it may change some unfavourable properties of included guest molecules. βCD protects drugs from biodegradation; exhibits high thermal stability; with a decomposition temperature close to 300 °C; is stable at basic and neutral pH; prevents the instability of molecules upon exposure to oxygen, water, radiation, heat or internal chemical reactions; reduces irritation caused by the direct entry of some medications to the body; and avoids incompatibility between drugs with other inactive ingredients (Del Valle, 2004; Tiwari et al., 2010). Indeed, the inclusion process may decrease the toxicity and increase the water solubility of drugs. Therefore, inclusions can be used to administer drugs to the body, transport them to the site of action of stably, and release them uniformly over long periods (Loftsson, Vogensen, Brewster, & Konrádsdóttir, 2007; Laza-Knoerr, 2010).

In terms of drug delivery, several works have addressed the inclusion processes of drugs in different CDs (Challa, Ahuja, Ali, & Khar, 2005; Priotti et al., 2015), but the main research interest has focused on increasing their solubility (Crestani, Azevedo, Veiga, & Gomez, 2011; Loftsson & Brewster, 1996). In comparison, little research has been devoted to the relationship and interplay between the solubility and the permeability, which must be associated in order to maximize the overall absorption (Dahan & Miller, 2012). Besides this, only few works has focused on structural features of the guest in the matrix that allow new uses of these CDs, such as stabilizing agents of metal nanoparticles (NPs) or others (Barrientos, Allende, Orellana, & Jara, 2012; Jullian et al., 2015; Monteiro et al., 2017; Sierpe et al., 2015; Vasconcelos et al., 2016). However, studying the guest conformations, possible conformations present, and inclusion geometries may facilitate discussing the values of the association constants, assessing their stability or even elucidating the drug release mechanisms. It would, therefore, be interesting to examine the chemical equilibrium criteria of the inclusion complexes (ICs) and their degree of dissociation in solution. Indeed, this information would allow the interaction force between the matrix and the guest to be estimated. For example, for various organic molecules, theoretical and experimental studies have predicted that the functional groups of the guests may remain exposed (Barrientos, Yutronic, Muñoz, Silva, & Jara, 2009; Sierpe et al., 2015). Studies performed by our research group on the inclusion geometry in complexes using CDs have demonstrated that the presence of gold nanoparticles (AuNPs) can produce a partial displacement of the guest out of the matrix because of the interaction of the guests' functional groups with the metal surface, while the non polar region remains included. Considering possible drug delivery applications, this phenomenon favours the controlled release of drugs during laser irradiation of the AuNPs (Sierpe et al., 2015).

AuNPs can be used to improve drug release and can be easily functionalized with diverse CD-based complexes for potential biomedical applications, including cancer treatments (Heo et al., 2012; Park et al., 2009; Shi, Goodisman, & Dabrowiak, 2013). In general, NPs offer strategies for more specific therapies; their small sizes allow them to penetrate cell membranes, improve targeting and increase the local concentration (De Jong & Borm, 2008). Among the widely diverse metal NPs, research into AuNPs has grown steadily because of their broad spectrum of bioapplications. For example, gold nanospheres with sizes between 4 and 100 nm have been shown to have low cytotoxicity (Connor, Mwamuka, Gole, Murphy, & Wyatt, 2005; Pan et al., 2007; Tirelli, 2006; Yen, Hsu, & Tsai, 2009). Additionally, they can act as nano-vehicles to transport and then release drugs in a sustained and controlled manner (Bansal et al., 2005; Dykman & Khlebtsov, 2012; Sonavane, Tomoda, & Makino, 2008). AuNPs also have notable optical properties; for example, they can absorb and release energy in a localized manner due to the resonant oscillations of free electrons in the conduction band. This process is called the photothermal effect and may be used as a strategy to destroy cancer cells, while releasing drug molecules, thereby providing additional therapeutic benefit (Bayazitoglu, Kheradmand, & Tullius, 2013; Choi et al., 2011; Guerrero et al., 2014; Jing-Liang and Gu, 2010). NPs accumulate preferentially in tumour sites due to the nature of these cells, enabled by the so-called enhanced permeability and retention (EPR effect). Structures of certain sizes tend to accumulate in tumour tissues substantially more than they do in normal tissues due to an increase in the production of blood vessels, extravasations and the lack of effective lymphatic drainage, among other factors. Therefore, biological processes can be influenced by nanometre-scale materials, which implies the potential for advances in the diagnosis and treatment of common diseases, such as cancer (Bertrand, Wu, Xu, Kamaly, & Farokhzad, 2014; Kobayashi, Watanabe, & Choyke, 2014; Nehoff, Parayath, Domanovitch, Taurin, & Greish, 2014).

The aim of this work is to construct a ternary system based on βCD and AuNPs that may be useful as a nanocarrier for different drugs, especially antineoplastic agents, which are poorly soluble, unstable and possess various therapeutic disadvantages, such as TG and MP. To this end, the complete characterization of the complexes obtained, the inclusion geometry and their interaction with AuNPs for potential application in drug release was achieved.

2. Materials and methods

2.1. Reagents and solvents

βCD hydrate (98% purity, 1134.98 g/mol), TG (> 98% purity, 167.2 g/mol) and MP monohydrate (> 98% purity, 170.2 g/mol) were

provided by Sigma-Aldrich Co. Ammonium hydroxide solution (28.0–30.0% NH_3) provided by Sigma-Aldrich Co and Milli-Q water (18 MΩ Millipore Nanopure purification system) were used as solvent. To obtain the AuNPs *via* magnetron sputtering a gold foil of high purity (99.9%) was used as precursor.

2.2. Synthesis of the ICs

To form the βCD-TG complex in a molar relation 1:1, 50.0 mg of TG were dissolved in water and 100 μL of ammonia, with constant stirring at 30 °C for 12 h. In addition, 339.4 mg of βCD were dissolved in water with constant stirring for 2 h at room temperature. Both solutions were cooled at 4 °C, and then mixed with gentle and constant stirring for 6 h, allowing the temperature to rise until slowly reach room temperature. The mixture was covered and kept motionless under a hood for 3 weeks. Crystals precipitated at the bottom of the solution were extracted before the complete evaporation of the solvents. An analogous procedure to obtain crystals of the βCD-MP complex was performed using 50.0 mg of MP and 333.7 mg of βCD.

2.3. Formation of AuNPs

AuNPs were obtained using magnetron sputtering under high vacuum with a Magnetron Sputter Coater PELCO SC-6. To deposit the NPs, crystalline powders of the βCD-TG and βCD-MP complexes were used as substrate (20 mg approximately). A gold foil was placed inside the vacuum chamber at 0.5 mbar, under inert atmosphere of argon. To begin the process, a current of 25 mA was used to ionize the gas, hitting the metal foil and release Au atoms. These Au atoms were deposited onto the crystal faces of βCD-TG and βCD-MP forming the AuNPs.

2.4. Powder X-ray diffractometry (PXRD)

The study was performed using a Siemens D-5000 diffractometer with graphite-monochromated Cu Kα radiation at 40 kV and 30 mA with a wavelength of 1.540598 Å. Previously; the crystals were dried and pulverized. The physical mixtures of βCD with TG or MP were performed at the molar ratio 1:1.

2.5. Thermogravimetric analysis (TGA)

Experiments were performed using a Perkin-Elmer Model 4000. The temperature of the furnace was programmed to rise at a rate of 10 °C/min from 30 °C to 800 °C under an air atmosphere (flow of 20 mL/min).

2.6. Nuclear magnetic resonance (NMR) spectroscopy

^{1}H NMR and rotating-frame Overhauser spectroscopy (ROESY) measurements were performed at 300 K on a Bruker Advance 400 MHz superconducting NMR spectrometer. The samples were dissolved in DMSO-d_6 (99.99% D). 2D NMR spectra were obtained using pulsed field gradient-selected methods during a mixing time of 12 h. Additionally, the stoichiometry of the complexes was evaluated by the integration of the protons signals of the βCD and the guests.

2.7. Phase solubility studies

The association constants of the complexes in water were obtained *via* phase solubility method using a PerkinElmer UV–vis Lambda 25 spectrophotometer (more details are given in the Supplementary material, Section S6).

2.8. Theoretical calculation

The electronic structure studies were performed using the conceptual framework of Density Functional Theory (DFT) incorporated in the Gaussian09 code. The DFT calculations were performed using the Becke's three-parameter exchange functional with Lee–Yang–Parr correlation functional (Becke, 1993). The continuum solvent model IEF-PCM was employed to represent the solvation effects (Cancès, Mennucci, & Tomasi, 1997; Cancès and Mennucci, 1998; Mennucci, Cancès, & Tomasi, 1997).

The stability of TG and MP tautomers was evaluated using the B3LYP/6-31 + g(d,p)/IEF-PCM (DMSO) theory level, considering Gibbs free energies (ΔG) and electronic energies (EE) theoretical calculations, in solution. Relative energies of the tautomers were calculated by comparison the lowest energy conformer. The populations were weighted considering the Boltzmann's distribution function, ΔG and EE. Boltzmann's distribution was discussed as probability of each conformer p_i.

$$pi = \frac{Ni}{N} = \frac{e^{-Ei/KT}}{\sum_i^j e^{-Ej/KT}}$$

Calculations *via* Autodock4.2 (Morris et al., 2009) were used to obtain the binding energy (BE) between TG and MP with βCD. TG and MP tautomers included in βCD were selected considering the most stable populations. These structures were employed to rationalize the experimental results. More details are given in the Supplementary material, Sections S2 and S7.

2.9. UV–vis spectroscopy in the solid state

AuNPs deposited onto the complexes were characterized by UV–vis absorption spectra in the solid state *via* diffuse reflectance measured using a Shimadzu UV 2450 spectrophotometer with barium sulfate as a baseline. Additionally, βCD-TG and βCD-MP spectra were used as a second baseline. The absorbances were calculated using the Kubelka–Munk transformations.

2.10. Scanning and transmission electronic microscopy (SEM and TEM)

SEM images were obtained using a LEO 1420VP system equipped with an Oxford 7424 energy-dispersive X-ray spectrometer (EDX) at an accelerating voltage of 25 kV. Field emission SEM (FE-SEM) images were obtained using a Zeiss Leo Supra 35-VP at an accelerating voltage of 15 kV and 2 kV.

TEM was conducted using a JEOL JEM 1200 EX II instrument at an acceleration voltage of 80 kV. Samples were prepared by dispersing approximately 0.5 mg in 100 μL of isopropanol (30%). Then, 20 μL of the solution were deposited onto a copper grid with a continuous film of Formvar.

2.11. Parallel artificial membrane permeability assays (PAMPA)

Transwell plates were used with two types of well, one called donor (lower) and another called acceptor (upper), the latter has a semi-permeable membrane of polyvinylidene fluoride (PVDF). 4 μL of phosphatidylcholine in dodecane (20 mg/mL) were deposited onto PVDF membranes of the acceptor plate, leaving for 5 min until complete evaporation of the solvent. Subsequent, 300 μL of phosphate-buffered saline (PBS) at pH 7.4 were added. In the donor well 300 μL of sample (200 mg/mL) dissolved in PBS were deposited.

Solutions of thiopental (10 mg in 100 mL of PBS 10 mM) and Evans blue (200 mg in 100 mL of PBS 10 mM) were used as positive and negative controls, respectively. The donor well loaded with samples and controls; and the acceptor well with PBS were assembled and sealed using parafilm. PAMPA was performed in triplicate (n = 3), for 24 h at 37 °C with shaking at 300 rpm. UV–vis measurements were performed dissolving 200 μL of the samples with PBS to a volume of 1.0 mL.

The effective permeability (*Pe*) was determined using the following equation:

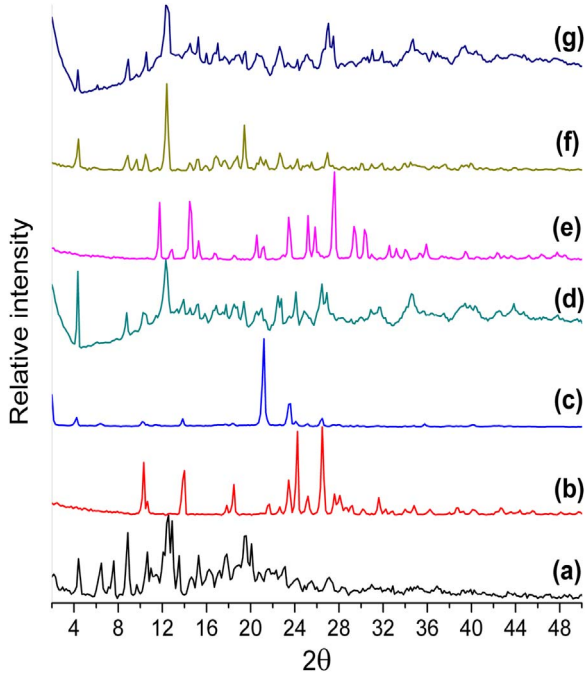

Fig. 2. Powder diffractograms of (a) pure βCD, (b) pure TG, (c) βCD-TG complex, (d) a physical mixture of βCD and TG, (e) pure MP, (f) βCD-MP and (g) a physical mixture of βCD and MP.

$$P_e = \frac{-218.3}{t} \cdot \log\left[1 - \frac{2 \cdot C_A(t)}{C_D(0)}\right] \cdot 10^{-6} \text{cm/s}$$

Where:

t = measurement time in hours.
C_A = concentration in the acceptor plate at time t.
C_D = concentration in the donor plate at time zero.

3. Results and discussion

3.1. Formation of the ICs

The diffraction patterns of the βCD matrix, the guests (TG and MP) and the ICs formed were obtained using PXRD (Fig. 2). The diffractograms of physical mixtures of pure species were also registered. The differences between the diffraction patterns observed for pure species and the complexes (*i.e.*, the disappearance of characteristic peaks and the appearance of new peaks) implied that the crystal packing arrangements of the ICs were different and, therefore, represented new crystalline phases (Caira, 2001; Dang et al., 2011).

The formation of the βCD-TG complex in the solid state was confirmed; the diffractometric trace (c) showed an intense peak at 20° for 2θ due to the inclusion of TG into βCD and differed from the trace obtained for the pure species. Similarly, the differences between the traces of βCD-MP (f) and those of βCD (a) and MP pure (e) demonstrated the effective inclusion of MP in the matrix. The diffraction patterns of βCD-TG, βCD-MP and the physical mixtures of their components were also compared (traces d and g); the differences in each trace showed that the crystalline powders obtained corresponded only to the complexes and not to the precipitates of their pure species.

TGA were performed to corroborate the formation of the ICs in the solid state through the mass losses according to the temperature changes. The results demonstrate that the drugs were included within the matrix with a completely displacing water molecules present. Moreover, the decomposition temperature of the drugs into the CD is less compared to the temperature of the free drugs. This was probably due to the fact that the crystalline packing of the pure drugs has higher energy interactions than the interactions of each drug with the inside the matrix (more details are given in the Supplementary material, Section S1).

Theoretical and experimental studies have reported the existence of four tautomeric species of TG and MP (Latosinska, Seliger, Zagar, & Burchardt, 2009). Nevertheless, it is possible to consider other conformations of these molecules with hydrogen atoms in different positions in their respective structures. The four additional conformations proposed in this work include the rotability of the thiol group and protonation of the N-3 atom.

To evaluate the stability of each tautomeric form, theoretical studies were performed using the DFT framework and DMSO as the solvent. ΔG and EE were obtained and employed to analyse the eight main conformations of the drugs; then, the Boltzmann's distribution function was applied. Fig. 3 shows all the tautomeric species obtained, and a summary of the energetic parameters calculated is presented in the Supplementary material (Section S2). Considering these results, in the case of TG, tautomers C (51.80%) and D (48.15%) were the most stable species. Meanwhile, for MP, tautomers D (80.23%) and C (19.76%) were the most stable, in solvent phase, due to the presence of a C=S double bond; and the proton movement from position 7 to 9 in both cases. The third place is occupied by the tautomer F with population 10–1000 times higher than the traditional conformations A and B. This is a first approach that includes these tautomeric forms. Energetic analysis suggests that these tautomeric forms should be considered in later studies.

NMR studies were conducted to demonstrate the stability of the complexes in solution, their stoichiometry and their inclusion geometries. ^{1}H NMR spectra of βCD, TG and MP were registered (see Supplementary material, Section S3). The proton spectrum of pure TG was not fully resolved, due to a polymerization of these molecules. The result was in agreement with theoretical and experimental studies that showed the presence of vertical stacking between the parallel bases of TG molecules generated by π–π interactions. Furthermore, these molecules can interact *via* hydrogen bonds, leading to the formation of pentamers (Latosinska et al., 2009). Fig. 4(a) shows the spectrum of the βCD-TG complex, which was probably resolved because of the inclusion phenomenon. No stacking π–π interactions between TG molecules occurred since the drug molecules were included in the βCD matrix and were, therefore, isolated from each other.

The chemical shift data of free TG, free βCD, and the IC are shown in Table 1 and demonstrate the effective inclusion of the drug in the matrix. The proton assignments of βCD, TG and MP molecules are shown in Fig. 1. For the assignment of the signals in the spectrum of the βCD-TG complex, theoretical calculations of the chemical shifts of the two most likely species of TG (conformations C and D) were performed (see the Supplementary material, Section S4). The calculated chemical shifts of OH-2, OH-3 and OH-6 hydroxyls towards higher field strengths indicated interactions with regions of TG that contributed electronic density; these displacements could also be due to interactions between the hydroxyl groups of neighbouring βCD molecules. Additionally, the chemical shifts of H-3 and H-5 protons of βCD indicated that the drug heterocycle was oriented towards the wider opening. The H′-8 and NH_2′ protons of TG also exhibited chemical shifts due to the inclusion phenomenon, which were different for each tautomeric species.

Fig. 4(b) shows the spectrum of the βCD-MP complex. Table 2 presents the chemical shifts of the IC formed with respect to those of pure βCD and MP. To assign the signals in the spectrum of the βCD-MP complex, theoretical calculations of the chemical shifts of the most stable tautomer of MP (conformation D) were performed because the experimental spectrum did not show other tautomeric forms (see the Supplementary material, Section S4). The chemical shifts of the H-3 and H-5 protons indicated a change in the chemical environment, which can be attributed to the inclusion of the drug, near the wider opening. An overlap in the proton signals of the OH-2 and OH-3 hydroxyls of the matrix is evident, whereas the proton signal of the OH-6 hydroxyl

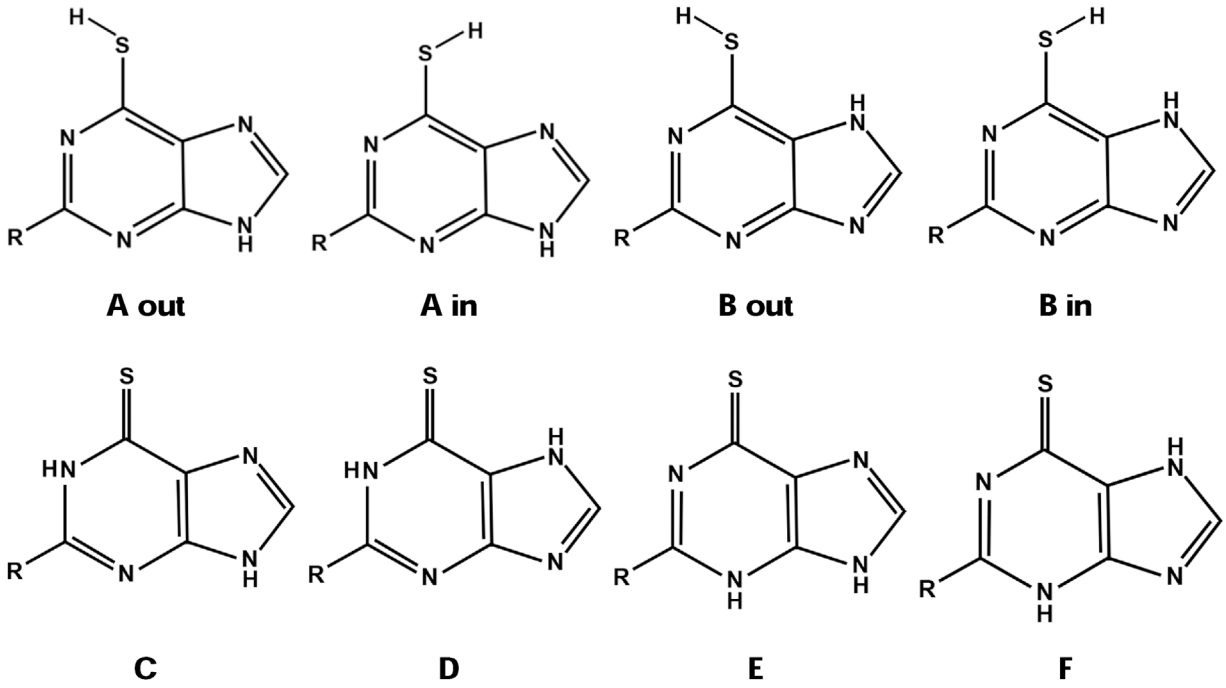

Fig. 3. Tautomeric structures of TG (R = NH_2) and MP (R = H).

broadened. These changes may be attributed to the formation of βCD dimers in solution. The chemical shifts of the protons of MP were also evaluated, which highlighted shifts towards low field strengths for protons H′-1/H′-7 in the heterocycle.

Integrating the proton signals of βCD as the matrix and each drug as a guest in the ^{1}H NMR spectra of the IC allowed for the determination of

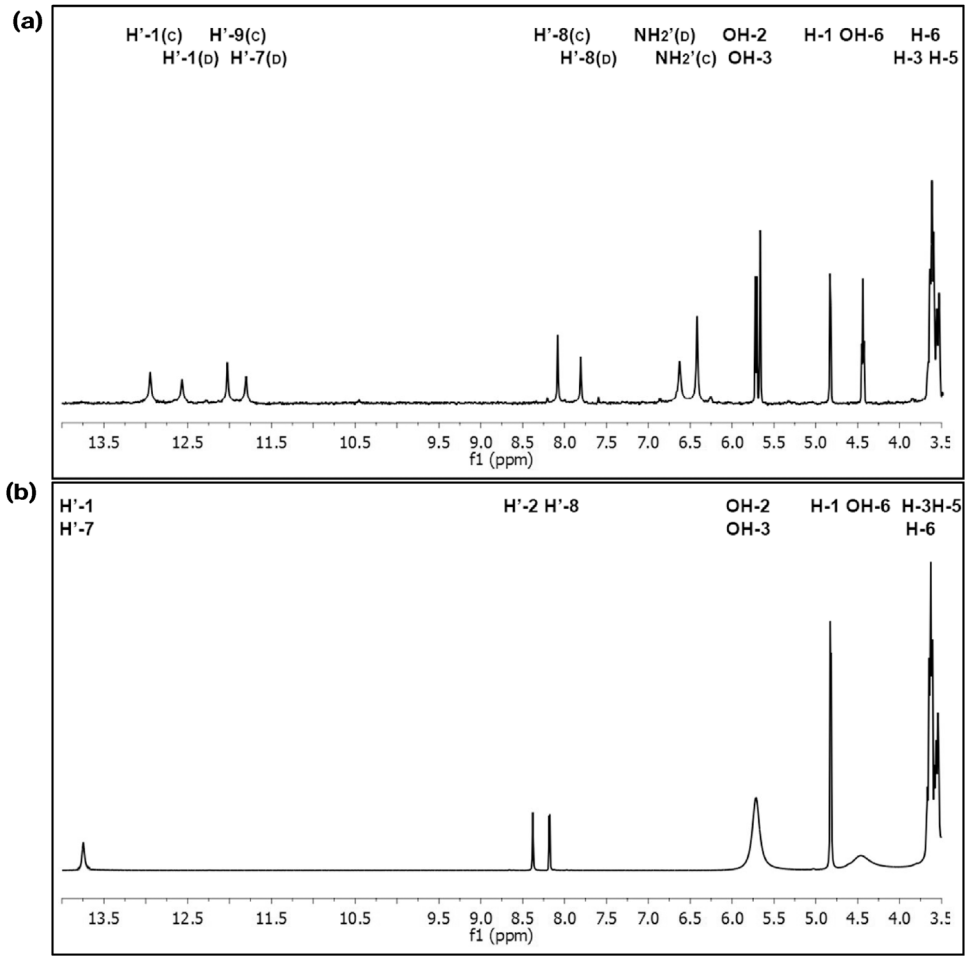

Fig. 4. ^{1}H NMR spectra of the (a) βCD-TG and (b) βCD-MP complexes.

Table 1
Chemical shifts of the βCD-TG complex and free species.

H of βCD	δ βCD (ppm)	δ βCD-TG (ppm)	Δδ (ppm)
H-3	3.648	3.676	0.028
H-5	3.555	3.568	0.013
H-6	3.617	3.624	0.007
OH-2	5.735	5.714	−0.021
OH-3	5.680	5.671	−0.009
OH-6	4.479	4.438	−0.041
H' of TG	**δ TG (ppm)**	**δ βCD-TG (ppm)**	**Δδ (ppm)**
H'-1(C)	–	12.947	–
H'-1(D)	–	12.569	–
H'-7(D)	–	12.025	–
H'-9(C)	–	11.803	–
NH2'(D)	6.566	6.626	0.060
NH2'(C)	6.449	6.418	−0.031
H'-8(C)	8.068	8.081	0.013
H'-8(D)	7.835	7.806	−0.029

Table 2
Chemical shifts of the βCD-MP complex and free species.

H de βCD	δ βCD (ppm)	δ βCD-MP (ppm)	Δδ (ppm)
H-3	3.648	3.668	0.020
H-5	3.555	3.580	0.025
H-6	3.617	3.620	0.003
OH-2	5.735	5.715	−0.020
OH-3	5.680	5.715	0.035
OH-6	4.479	4.463	−0.016
H' de MP	**δ MP (ppm)**	**δ βCD-MP (ppm)**	**Δδ (ppm)**
H'-2	8.373	8.382	0.009
H'-1/H'-7	13.723	13.747	0.024
H'-8	8.176	8.178	0.002

the stoichiometry of each system in solution according to a methodology used for different CD complexes (Barrientos et al., 2009; Rodriguez-Llamazares et al., 2007). The integration of the H-1 proton of the matrix was used as a reference and compared with results of integrating the resolved signals of the protons of TG and MP. Specifically, in the βCD-TG complex, the H′-8 protons of the two observed tautomeric species of TG were integrated, whereas in the βCD-MP complex, the H′-8 proton of MP was integrated. The stoichiometric matrix:guest ratio calculated for both complexes was 1:1 (more details are given in the Supplementary material, Section S5).

ROESY studies have been used frequently to analyze supramolecular systems based in CDs. Moreover, this technique can be used to evaluate the geometric structures of ICs in solution with a high degree of precision (Pessine, Calderini, & Alexandrino, 2014, chap. 12; Schneider, Hacket, & Rudiger, 1998). ROESY was performed to determine interactions between the hydrogen nuclei of the guest with those of βCD (Bergonzi, Bilia, Di Bari, Mazzia, & Vincieri, 2007; Bisson-Boutelliez, Fontanay, Finance, & Kedzierewicz, 2010; Jahed, Zarrabi, Bordbar, & Hafezi, 2014; Voulgari, Benaki, Michaleas, & Antoniadou-Vyza, 2007).

The analysis showed the cross peaks produced by the interaction between the inner protons of βCD mainly with H′-8 and H′-1/H′-7 protons of MP, thus demonstrating the effective inclusion of the drug. Notably ROESY analysis showed the correlation between the H′-8 protons of MP with OH-2 and OH-3 hydroxyl group protons of the βCD, which implies that the drug is oriented towards the narrow of the truncated cone. The full ROESY spectrum and the specific interactions between βCD and MP are given in the Supplementary material, Section 4.

To study the inclusion geometries of the complexes, molecular modelling of the preferred tautomers of TG and MP included in the βCD was conducted. The model revealed a preferred orientation for each complex that was in good agreement with the experimental results obtained by NMR. Fig. 5 shows the complexes modelled using docking (right) and the proposed inclusion geometries for both complexes based on the chemical changes determined by NMR and modelling (left).

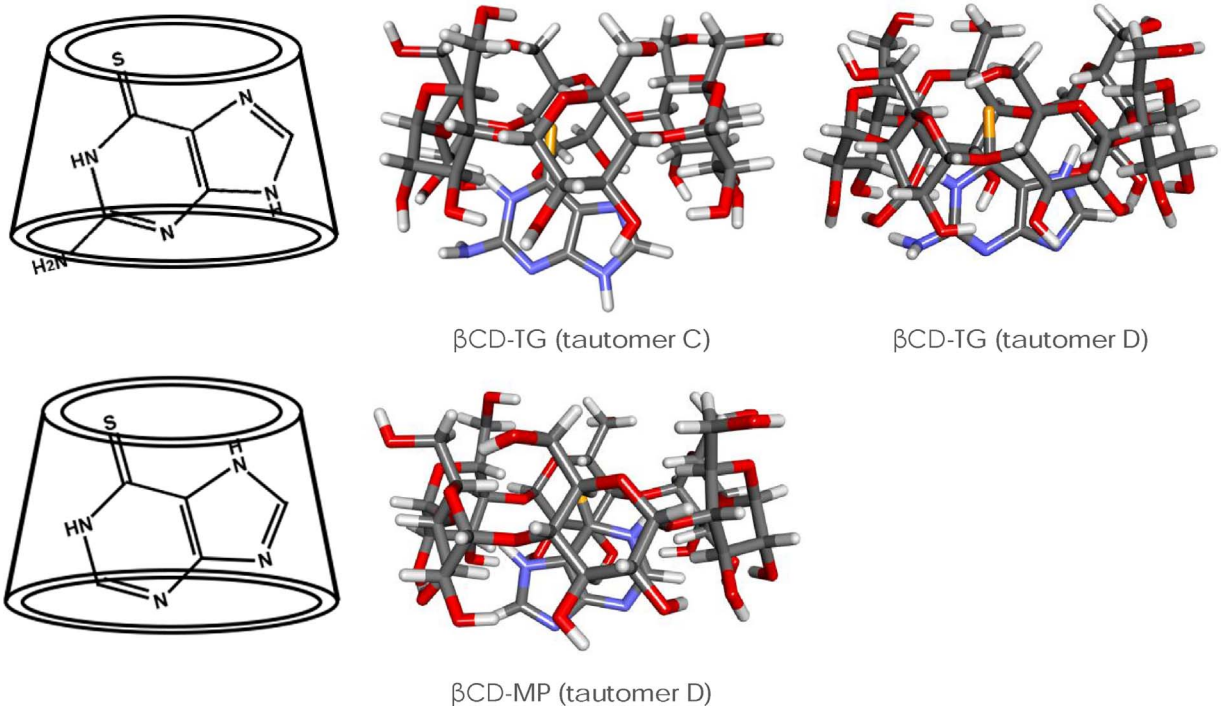

Fig. 5. Proposed inclusion geometries of βCD-TG (up) and βCD-MP (down).

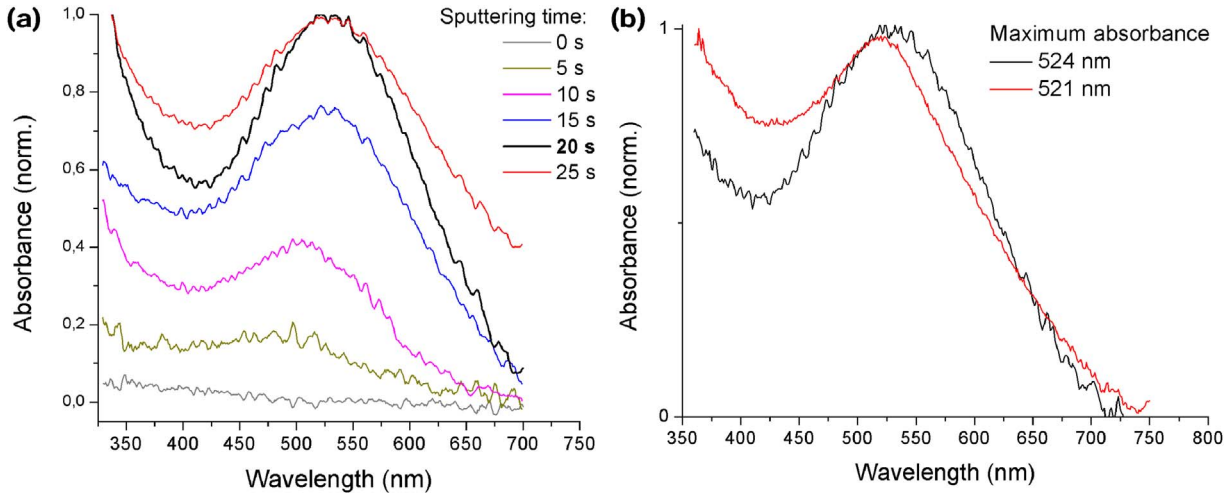

Fig. 6. Optical spectra of (a) AuNPs on microcrystals of βCD-TG with different sputtering exposure times and (b) AuNPs on microcrystals of βCD-TG (black line) and βCD-MP (red line) exposed to sputtering for 20 s. (For interpretation of the references to colour in this figure legend, the reader is referred to the web version of this article.)

The association constants (K) of the βCD-TG and βCD-MP complexes were determined by UV–vis spectroscopy using the phase solubility method (Connors, 1997; Higuchi and Connors, 1965). First, the molar extinction coefficient (ε) was obtained for each drug dissolved in water, and then, the respective constants were calculated. The value of βCD-TG was 261 M^{-1} and of βCD-MP was 368 M^{-1}. Generally, the K values of complexes of βCD with different drugs should vary between 50 and 2000 M^{-1} for biological applications (Connors, 1997; Rao & Stella, 2003), therefore the values obtained of both ICs were suitable for drug delivery purposes. More details can be found in the Supplementary material (Section S6).

3.2. Formation of the ternary system

UV–vis spectroscopy studies performed in the solid state confirmed the effective deposition of metal NPs onto crystals of the IC. Fig. 6(a) shows the spectra obtained after different exposure times of the complexes to sputtering. Periods of 5 s were applied to achieve an optimum ratio between the absorption intensity and band width in the spectra, which was reached in the first 20 s of exposure. Fig. 6(b) shows the UV–vis spectra of AuNPs on crystalline powders of βCD-TG and βCD-MP with absorption maxima of 524 nm and 521 nm, respectively, obtained after 20 s of magnetron sputtering.

FE-SEM allowed the AuNPs deposited on the crystalline powder of the IC studied to be observed directly. Additionally, EDX was performed to confirm the presence of Au deposited on the crystals in addition to the characteristic elements C, O and S of the complexes (Fig. 7). Finally, diverse SEM images of βCD, TG, MP, βCD-TG and βCD-MP were obtained to show the crystal morphologies of the ICs formed and compare them with those of their pure components (see the Supplementary material, Section S8).

TEM was conducted to determine the average sizes of the AuNPs obtained from sputtering for 20 s (see the Supplementary material, Section S9). The ternary systems of βCD-TG-AuNPs and βCD-MP-AuNPs in the solid state were dissolved, and the AuNPs were recovered with the complexes forming a stable colloidal solution. The AuNPs covered with βCD-TG had an average diameter of 23 nm (± 5), and the AuNPs covered with βCD-MP had an average diameter of 21 nm (± 3) based on their respective statistical analyses.

3.3. Permeability studies using artificial membranes

PAMPA evaluates the ability of a compound to spread between plates separated by a phosphatidylcholine filter, which acts as a lipid membrane and simulates the lipid bilayers of different cell types. Since artificial membranes contain no active transport system or metabolic enzymes, only the passive diffusion of species can be studied using this technique (Kansy, Senner, & Gubernator, 1998; Ottaviani, Martel, & Carrupt, 2006). PAMPA was performed for pure species and complexes formed with and without AuNPs.

Under certain conditions, the CDs can improve drug permeation through biological membranes. This depends on factors such as the unstirred water layer formed on the phospholipid surface, stirring rate, type of CD or complexation affinity, among others (Brewster, Noppe, Peeters, & Loftsson, 2007; Loftsson et al., 2007). The results obtained (Fig. 8) demonstrated that TG and MP included in βCD exhibited increased effective permeability, which is relevant to improve the cell penetration of these antitumour drugs. In contrast, the AuNPs did not have the capacity to diffuse through the membrane by passive diffusion (Wang, Lee, Chiou, & Wei, 2010; Moser et al., 2016). The ternary systems of AuNPs-βCD-TG and AuNPs-βCD-MP possessed low effective permeabilities under the studied conditions. Therefore, formation of ternary systems between ICs and AuNPs avoid the passive diffusion by a membrane, giving the possibility to gather the release of ICs with a laser by photothermal effect which would allow a controlled spatial and temporal drug delivery. All absorbances and concentration values obtained can be found in the Supplementary material (Section S10).

4. Conclusions

Two ternary systems composed of βCD, TG and MP, and AuNPs were designed. The complexes of βCD-TG and βCD-MP were formed reproducibly in the solid state at a molar ratio of 1:1 and remained stable after being dissolved. The association constants of the βCD-based complexes were suitable for pharmaceutical uses. The most stable species of TG were tautomers C and D, whereas for MP, the most stable species was tautomer D; these species were partially included in the interior of the βCD, leaving their functional groups exposed and, thus, allowing for the deposition of AuNPs.

The ternary systems βCD-TG-AuNPs and βCD-MP-AuNPs were

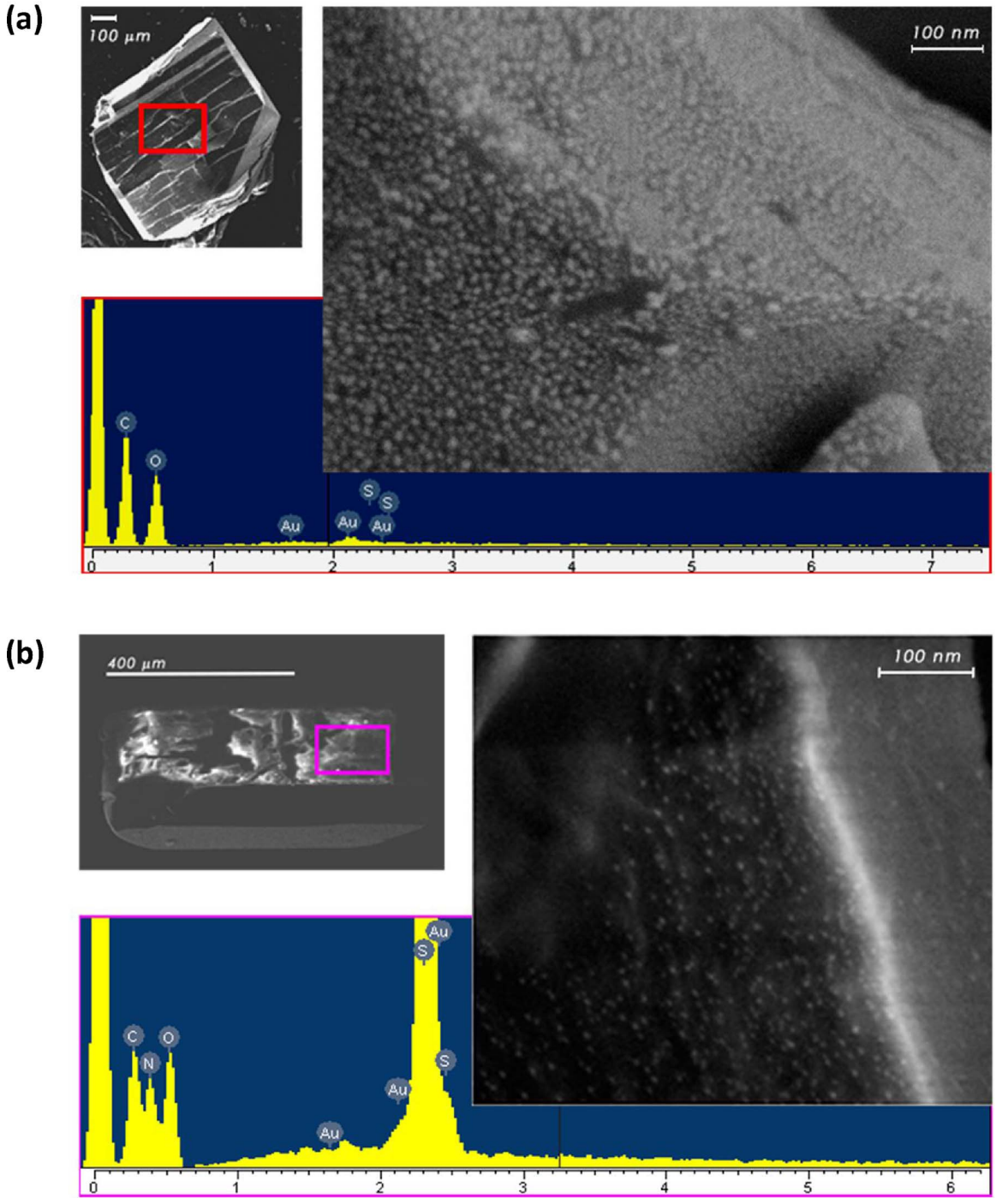

Fig. 7. FE-SEM images of a crystal of (a) βCD-TG with AuNPs and (b) βCD-MP with AuNPs and their respective EDX results.

formed in the solid state. Then, they were dissolved, and the AuNPs covered by the complexes were solution stable and had diameters of 23 nm and 21 nm, respectively. The nanometric sizes of these ternary systems were consistent with those reported in the literature for metal NPs that are not toxic to organisms. PAMPA revealed an increase in the effective permeability using βCD and demonstrated that systems containing AuNPs did not diffuse through the membrane *via* passive diffusion, which favours their controlled release.

We designed these systems to include antitumour drugs; however, they can be applied to any drug with adequate dimensions that currently exhibit therapeutic disadvantages. The ternary systems increased the solubility of TG and MP and could improve their delivery to the site of action, among other advantages in the field of drug delivery.

Acknowledgments

R. Sierpe thanks CONICYT by the fellowship of PhD [21100442]. This study was funded for FONDECYT [1160114, 1170929, and 1171654], FONDEQUIPEQM140174 and FONDAP [15130011]. Thanks to Dassault Systèmes BIOVIA, Discovery Studio Modeling Environment, Release 2017, San Diego: Dassault Systèmes, 2016 by the quality images obtained by docking. Dr. María Luisa Valenzuela V., Director Institute of Applied Chemical Sciences, Universidad Autónoma de Chile by conduct the TGA analyzes, and Erika Lang for her help in the development of ROESY spectra.

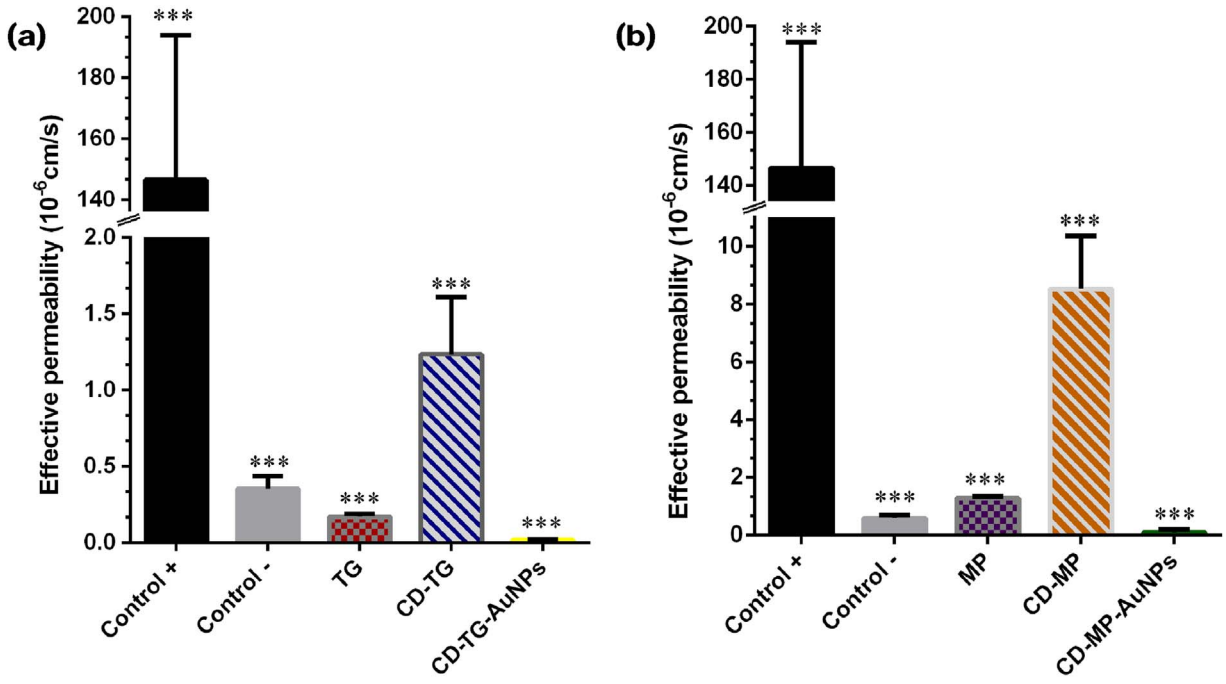

Fig. 8. Effective permeabilities of (a) free TG, TG with βCD, and TG with βCD and AuNPs, and (b) free MP, MP with βCD, and MP with βCD and AuNPs. Thiopental and Evans Blue solutions were used as negative and positive controls, respectively. The assays were performed at 37 °C for 24 h, using PBS as solvent, (n = 3).

Appendix A. Supplementary data

Supplementary data associated with this article can be found, in the online version, at http://dx.doi.org/10.1016/j.carbpol.2017.08.102.

References

Barrientos, L., Yutronic, M., Muñoz, M., Silva, N., & Jara, P. (2009). Metallic nanoparticle tropism of alkylthiol guest molecules included into α-cyclodextrin host. *Supramolecular Chemistry, 21*, 264–267.

Barrientos, L., Allende, P., Orellana, C., & Jara, P. (2012). Ordered arrangements of metal nanoparticles on alpha-cyclodextrin inclusion complexes by magnetron sputtering. *Inorganica Chimica Acta, 380*, 372–377.

Bayazitoglu, Y., Kheradmand, S., & Tullius, T. K. (2013). An overview of nanoparticle assisted laser therapy. *International Journal of Heat and Mass Transfer, 67*, 469–486.

Becke, A. D. (1993). Density-functional thermochemistry. III. The role of exact exchange. *Journal of Chemistry Physics, 98*(7), 5648–5652.

Bergonzi, M., Bilia, A., Di Bari, L., Mazzia, G., & Vincieri, F. (2007). Studies on the interactions between some flavonols and cyclodextrins. *Bioorganic & Medicinal Chemistry Letters, 17*, 5744–5748.

Bertrand, N., Wu, J., Xu, X., Kamaly, N., & Farokhzad, O. (2014). Cancer nanotechnology: The impact of passive and active targeting in the era of modern cancer biology. *Advance Drug Delivery Reviews, 66*, 2–25.

Bisson-Boutelliez, C., Fontanay, S., Finance, C., & Kedzierewicz, F. (2010). Preparation and physicochemical characterization of amoxicillin β-cyclodextrin complexes. *American Association of Pharmaceutical Scientists PharmSciTech, 11*(2), 574–581.

Bohon, J., & De los Santos, C. (2003). Structural effect of the anticancer agent 6-thioguanine on duplex DNA. *Nucleic Acids Research, 31*(4), 1331–1338.

Brewster, M., Noppe, M., Peeters, J., & Loftsson, T. (2007). Effect of the unstirred water layer on permeability enhancement by hydrophilic cyclodextrins. *International Journal of Pharmaceutics, 342*, 250–253.

Caira, M. R. (2001). On the isostructurality of cyclodextrin inclusion complexes and its practical utility. *Revue Roumaine de Chimie, 46*, 371–386.

Cancès, E., & Mennucci, B. (1998). Nes applications of integral equations methods for solvatation continuum models: Ionic solutions and liquid crystals. *Journal of Mathematical Chemistry, 23*, 309–326.

Cancès, E., Mennucci, B., & Tomasi, J. (1997). A new integral equation formalism for the polarizable continuum model: Theoretical background and applications to isotropic and anisotropic dielectrics. *Journal of Chemistry Physics, 107*(8), 3032–3041.

Ceborska, M. (2014). Interactions of native cyclodextrins with biorelevant molecules in the solid state: A review. *Current Organic Chemistry, 18*, 1878–1885.

Challa, R., Ahuja, A., Ali, J., & Khar, R. K. (2005). Cyclodextrins in drug delivery: An updated review. *American Association of Pharmaceutical Scientist, 6*(2), 43.

Chande, N., Townsend, C. M., Parker, C. E., & MacDonald, J. K. (2016). Azathioprine or 6-mercaptopurine for induction of remission in Crohn's disease. *Cochrane Database of Systematic Reviews*, 1–66.

Chen, W., Chang, C. E., & Gilson, M. K. (2004). Calculations of cyclodextrin binding affinities: Energy, entropy and implications for drug design. *Biophysical Journal, 87*(5), 3035–3049.

Chen, M., Diao, G., & Zhang, E. (2006). Study of inclusion complex of β-cyclodextrin and nitrobenzene. *Chemosphere, 63*, 522–529.

Choi, J., Yang, J., Jang, E., Suh, J. S., Huh, Y. M., Lee, K., et al. (2011). Gold nanostructures as photothermal therapy agent for cancer. *Anti-Cancer Agents in Medicinal Chemistry, 11*(10), 953–964.

Connor, E., Mwamuka, J., Gole, A., Murphy, C. J., & Wyatt, M. D. (2005). Gold nanoparticles are taken up by human cells but do not cause acute cytotoxicity. *Small, 1*, 325–327.

Connors, K. A. (1997). The stability of cyclodextrin complexes in solution. *Chemical Reviews, 97*, 1325–1357.

Crestani, J., Azevedo, T., Veiga, F., & Gomez, H. (2011). Cyclodextrins and ternary complexes: Technology to improve solubility of poorly soluble drugs. *Brazilian Journal of Pharmaceutical Sciences, 47*, 665–681.

Dahan, A., & Miller, J. (2012). The solubility–permeability interplay and its implications in formulation design and development for poorly soluble drugs. *American Association of Pharmaceutical Scientists PharmSciTech, 14*(2), 244–251.

Dang, Z., Song, L. X., Guo, X. Q., Du, F. Y., Yang, J., & Yang, J. (2011). Applications of powder X-ray diffraction to inclusion complexes of cyclodextrins. *Current Organic Chemistry, 15*, 848–861.

De Jong, W., & Borm, P. (2008). Drug delivery and nanoparticles: Applications and hazards. *International Journal of Nanomedicine, 3*, 133–149.

Del Valle, E. M. M. (2004). Cyclodextrins and their uses: A review. *Process Biochemistry, 39*, 1033–1046.

Douhal, A. (2004). Ultrafast guest dynamics in cyclodextrin nanocavities. *Chemical Reviews, 104*, 1955–1976.

Dykman, L., & Khlebtsov, N. (2012). Gold nanoparticles in biomedical applications: Recent advances and perspectives. *Chemical Society Reviews, 41*, 2256–2282.

Elion, G. B. (2008). The purine path to chemotherapy. *Science, 244*(4900), 41–47.

Erb, N., Harms, D. O., & Janka-Schaub, G. (1998). Pharmacokinetics and metabolism of thiopurines in children with acute lymphoblastic leukemia receiving 6-thioguanine versus 6-mercaptopurine. *Cancer Chemotherapy and Pharmacology, 42*, 266–272.

Gidwani, B., & Vyas, A. (2015). A comprehensive review on cyclodextrin-based carriers for delivery of chemotherapeutic cytotoxic anticancer drugs. *BioMed Research International, 15*, 1–15.

Guerrero, A., Hassan, N., Escobar, C., Albericio, F., Kogan, M. J., & Araya, E. (2014). Gold nanoparticles for photothermally controlled drug release. *Nanomedicine, 13*, 2023–2029.

Heo, D., Yang, D., Moon, H., Lee, J., Bae, M., Lee, S., et al. (2012). Gold nanoparticles surface-funcionalized with paclitaxel drug and biotin receptor as theranostic agents for cancer therapy. *Biomaterials, 33*(3), 856–866.

Higuchi, T., & Connors, K. A. (1965). Phase solubility techniques. *Advances in Analytical Chemistry and Instrumentation, 4*, 117–122.

Jahed, V., Zarrabi, A., Bordbar, A., & Hafezi, M. (2014). NMR (1H, ROESY) spectroscopic and molecular modelling investigations of supramolecular complex of β-cyclodextrin and curcumin. *Food Chemistry, 165*, 241–246.

Jing-Liang, L., & Gu, M. (2010). Gold-nanoparticle-enhanced cancer photothermal therapy. *IEEE Journal of Selected Topics in Quantum Electronics, 16*(4), 989–996.

Jullian, C., Fernández-Sandoval, S., Celis-Barros, C., Abarca, B., Ballesteros, R., & Zapata-

Torres, G. (2015). Supramolecular assemblies of phenyl-pyridyl-triazolopyridine and β-cyclodextrin as sensor of divalent cations in aqueous solution. *Carbohydrate Polymers, 121*, 295–301.
Kansy, M., Senner, F., & Gubernator, K. (1998). Physico chemical high through put screening: Parallel artificial membrane permeation assay in the description of passive absorption processes. *Journal of Medicinal Chemistry, 41*(7), 1007–1009.
Kobayashi, H., Watanabe, R., & Choyke, P. (2014). Improving conventional enhanced permeability and retention (EPR) effects; what is the appropriate target? *Theranostics, 4*, 81–89.
Krynetskaia, N. F., Feng, J. Y., Krynetski, E. Y., Garcia, J. V., Panetta, J. C., Anderson, K. S., et al. (2001). Deoxythioguanosine triphosphate impairs HIV replication: A new mechanism for an old drug. *The FASEB Journal, 15*, 1902–1908.
Latosinska, J., Seliger, J., Zagar, V., & Burchardt, D. V. (2009). Hydrogen bonding and stacking π-π interactions in solid 6-thioguanine and 6-mercaptopurine (antileukemia and antineoplastic drugs) studied by NMR-NQR double resonance spectroscopy and density functional theory. *The Journal of Physical Chemistry A, 113*, 8781–8790.
Laza-Knoerr, A. (2010). Cyclodextrins for drug delivery. *Journal of Drug Targeting, 18*, 645–656.
Loftsson, T., & Brewster, M. (1996). Pharmaceutical applications of cyclodextrins. 1. Drug solubilization and stabilization. *Journal of Pharmaceutical Science, 85*(10), 1017–1025.
Loftsson, T., & Brewster, M. (2010). Pharmaceutical applications of cyclodextrins: Basic science and product development. *Journal of Pharmacy and Pharmacology, 62*, 1607–1621.
Loftsson, T., Vogensen, S. B., Brewster, M. E., & Konrádsdóttir, F. (2007). Effects of cyclodextrins on drug delivery through biological membranes. *Journal of Pharmaceutical Sciences, 96*(10), 1532–1546.
Makedonopoulou, S., & Mavridis, I. (2000). Structure of the inclusion complex of β-cyclodextrin with 1,12-dodecanedioic acid using synchrotron radiation data; a detailed dimeric β-cyclodextrin structure. *Acta Crystallographica Section B Structural Science, B56*, 322–331.
Mennucci, B., Cancés, E., & Tomasi, J. (1997). Evaluation of solvent effects in isotropic and anisotropic dielectrics and in ionic solutions with a unified integral equation method: Theretical bases, computational implementation, and numerical applications. *Journal of Physical Chemistry B, 101*(49), 10506–10517.
Monteiro, A., Caminhas, L., Ardisson, J., Paniago, R., Cortés, M., & Sinisterra, D. (2017). Magnetic nanoparticles coated with cyclodextrins and citrate for irinotecan delivery. *Carbohydrate Polymers, 163*, 1–9.
Morris, G., Huey, R., Lindstrom, W., Sanner, M., Belew, R., Goodsell, D., et al. (2009). AutoDock4 and AutoDocktools4: Automated docking with selective receptor flexibility. *Journal of Computational Chemistry, 30*(16), 2785–2791.
Moser, F., Hildenbrand, G., Müller, P., Al Saroori, A., Biswas, A., Bach, M., et al. (2016). Cellular uptake of gold nanoparticles and their behavior as labels for localization microscopy. *Biophysical Journal, 110*, 947–953.
Nehoff, H., Parayath, H., Domanovitch, L., Taurin, S., & Greish, K. (2014). Nanomedicine for drug targeting: Strategies beyond the enhanced permeability and retention effect. *International Journal of Nanomedicine, 9*, 2539–2555.
Ottaviani, G., Martel, S., & Carrupt, P. A. (2006). Parallel artificial membrane permeability assay: A new membrane for the fast prediction of passive human skin permeability. *Journal of Medicinal Chemistry, 49*(13), 3948–3954.
Pan, Y., Neuss, S., Leifert, A., Fischler, M., Wen, F., Simon, U., et al. (2007). Size-dependent cytotoxicity of gold nanoparticles. *Small, 3*, 1941–1949.
Park, C., Youn, H., Kim, H., Noh, T., Hee, Y., Tax, E., et al. (2009). Cyclodextrin-covered gold nanoparticles for targeted delivery of an anti-cancer drug. *Journal of Materials Chemistry, 19*, 2310–2315.
Pessine, F., Calderini, A., & Alexandrino, G. (2014). Review: Cyclodextrin inclusion complexes probed by NMR techniques. In D. Kim (Ed.). *Magnetic resonance spectroscopy* (pp. 237–265). InTech.
Priotti, J., Ferreira, M. J., Lamas, C., Leonardi, D., Salomon, C., & Nunes, T. (2015). First solid-state NMR spectroscopy evaluation of complexes of benznidazole with cyclodextrin derivatives. *Carbohydrate Polymers, 131*, 90–97.
Rao, V., & Stella, V. (2003). When can cyclodextrins be considered for solubilizing purposes. *Journal of Pharmaceutical Sciences, 92*, 927–932.
Rodriguez-Llamazares, S., Jara, P., Yutronic, N., Noyong, M., Bretschneider, J., & Simon, U. (2007). Face preferred deposition of gold nanoparticles on α-cyclodextrin/octanethiol inclusion compound. *Journal of Colloid Interface Science, 316*, 202–205.
Schmiegelow, K., Nielsen, S., Frandsen, T., & Nersting, J. (2014). Mercaptopurine/methotrexate maintenance therapy of childhood acute lymphoblastic leukemia: Clinical facts and fiction. *Journal of Pediatric Hematology/Oncology, 36*(7), 503–517.
Schneider, H., Hacket, F., & Rudiger, V. (1998). NMR Studies of cyclodextrins and cyclodextrin complexes. *Chemical Reviews, 98*, 1755–1785.
Shi, Y., Goodisman, J., & Dabrowiak, J. (2013). Cyclodextrin capped gold nanoparticles as a delivery vehicle for a prodrug of cisplatin. *Inorganic Chemistry, 52*, 9418–9426.
Sierpe, R., Lang, E., Jara, P., Guerrero, A., Chornik, B., Kogan, M., et al. (2015). Gold nanoparticle interacting with β-cyclodextrin-phenylethylamine inclusión complex: A ternary system for photothermal drug release. *ACS Applied Materials & Interfaces, 7*(28), 15177–15188.
Sonavane, G., Tomoda, K., & Makino, K. (2008). Biodistribution of colloidal gold nanoparticles after intravenous administration: Effect of particle size. *Colloids and Surfaces B: Biointerfaces, 66*, 274–280.
Tirelli, N. (2006). (Bio)Responsive nanoparticles. *Current Opinion in Colloid & Interface Science, 11*, 210–216.
Tiwari, G., Tiwari, R., & Rai, A. K. (2010). Cyclodextrins in delivery systems: Applications. *Journal of Pharmacy and Bioallied Sciences, 2*(2), 72–79.
Vasconcelos, D., Kubota, T., Santos, D., Araujo, M., Teixeira, A., & Gimenez, I. (2016). Preparation of Au_n quantum clusters with catalytic activity in β-cyclodextrin polyurethane nanosponges. *Carbohydrate Polymers, 136*, 54–62.
Voulgari, A., Benaki, D., Michaleas, S., & Antoniadou-Vyza, E. (2007). The effect of β-cyclodextrin on tenoxicam photostability, studied by a new liquid chromatography method; the dependence on drug dimerisation. *Journal of Inclusion Phenomena and Macrocyclic Chemistry, 57*, 141–146.
Wang, S. H., Lee, C. W., Chiou, A., & Wei, P. K. (2010). Size-dependent endocytosis of gold nanoparticles studied by three-dimensional mapping of plasmonic scattering images. *Journal of Nanobiotechnology, 8*(33), 1–13.
Whang, H. S., Vendeix, F., Gracz, H., Gadsby, J., & Tonelli, A. (2007). NMR Studies of the inclusion complex of cloprostenol sodium salt with β-cyclodextrin in aqueous solution. *Pharmaceutical Research, 25*(5), 1142–1149.
Yen, H. J., Hsu, S. H., & Tsai, C. L. (2009). Cytotoxicity and immunological response of gold and silver nanoparticles of different sizes. *Small, 5*, 1553–1561.
Zhang, J. X., & Ma, P. X. (2013). Cyclodextrin-based supramolecular systems for drug delivery: Recent progress and future perspective. *Advanced Drug Delivery Reviews, 65*, 1215–1233.